Experimental modelling of flatness defects in strip cold rolling

Tran Dinh-Cuong, Nicolas Tardif, Ali Limam

▶ **To cite this version:**

Tran Dinh-Cuong, Nicolas Tardif, Ali Limam. Experimental modelling of flatness defects in strip cold rolling. ROLLING 2013, Jun 2013, Venice, Italy. hal-01863092

HAL Id: hal-01863092
https://hal.science/hal-01863092

Submitted on 28 Aug 2018

HAL is a multi-disciplinary open access archive for the deposit and dissemination of scientific research documents, whether they are published or not. The documents may come from teaching and research institutions in France or abroad, or from public or private research centers.

L'archive ouverte pluridisciplinaire **HAL**, est destinée au dépôt et à la diffusion de documents scientifiques de niveau recherche, publiés ou non, émanant des établissements d'enseignement et de recherche français ou étrangers, des laboratoires publics ou privés.

EXPERIMENTAL MODELLING OF FLATNESS DEFECTS IN STRIP COLD ROLLING

Tran Dinh Cuong[a], Nicolas Tardif[a], Ali Limam[a]

[a]Civil and Environmental Engineering Laboratory,
National Institute of Applied Sciences at Lyon,
Albert Einstein Avenue, Villeurbanne 69621, France

ABSTRACT

The manufacturing of sheet with a growing mechanical yield stress, a decreasing thickness and small flatness defects is a major challenge for the cold rolling of aluminum alloy or steel. Compressive residual stress may appear due to the manufacturing process and induce elastic wave buckling, responsible for flatness defects.
The study aims to analyse experimentally the interaction between residual stress and buckling in terms of mode and amplitude. The residual stress is simulated by thermal stress.
The custom test is able to reproduce usual rolling buckling modes (center wave, edge wave...). It is able to simulate "manifested" flatness defects (ie flatness defects during the tension of the strip) but also "latent" flatness defects (when defects show up after tension release).
Full field measurements of the temperature and the out-of-plane coordinate give high resolution inputs for numerical model validation.

KEYWORDS

Thermal buckling, Rolling, Flatness defect, Residual stress, Experiments, Modelling

INTRODUCTION

The manufacturing of sheet with a growing mechanical yield stress, a decreasing thickness and small flatness defects is a major challenge for the cold rolling of aluminum alloy or steel. Increasing forces during the rolling induce higher deformation of the rolls and consequently a heterogeneous thickness reduction over the width of the strip. Then compressive residual stress appears and elastic wave buckling can be expected at the edge or at the center of the strip (Fig. 1).

A lot of more or less simplified models are used to calculate the flatness defects in rolling. Some of them uncouple the buckling calculation from the calculation of the residual stress making the assumption that the buckling does not affect the stress distribution in the bite. [3, 4, 5] used analytical buckling calculation to estimate the intensity and the type of residual stress in the strip. [6] used the asymmptotic numerical method to calculate buckling and post-buckling of a laminated strip. [7] compared a technique using slowly variable Fourier coefficients and the asymmptotic Landau-Ginzburg approach to define simple macroscopic models describing the influence of local wrinkling on membrane behavior. A few of them couple the buckling calculation and the residual stress calculation [2, 1] using a simple macroscopic model [8] to take into account buckling.

To validate the models, an experimental study would be needed with accurate measurement of the residual stress distribution, buckling modes and amplitude. An in-situ instrumentation of the rolling mill is not suitable for a satisfactory control of the residual stress in the strip because they depend on

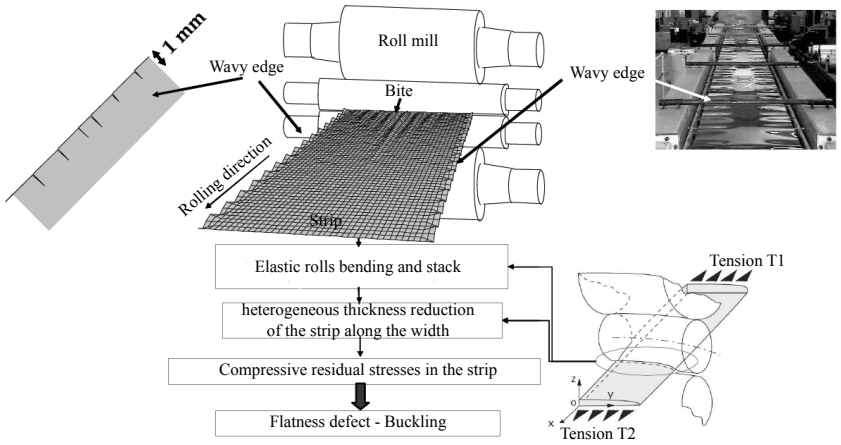

Fig. 1: Flatness defects in rolling [1]

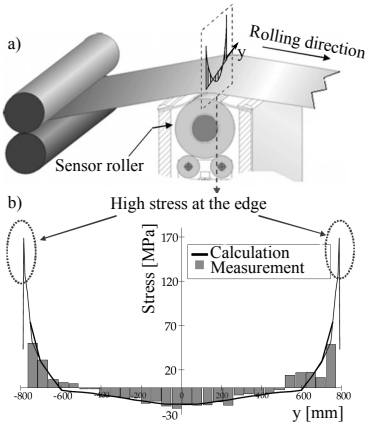

Fig. 2: Residual stress measurement by tensiometer rolls, a) Tensiometer rolls [1], b) Comparison of the measurement [2] and calculation (LAM3) [1]

several coupled physics (elastic-viscoplasticity, tribology, thermics...) [9, 10, 1].
Moreover, local residual stress distribution (for one absissa in the rolling direction) may be measured by tensiometer rolls but the resolution of the sensors in the transverse y-direction is not good enough for high stress gradient region (Fig. 2).

Hence, the study proposes a custom experimental setup to analyze the interaction between residual stress and buckling in terms of modes and amplitude. The stress distribution is simulated by a combination of a global mechanical tension and a non-uniform thermal stress distribution. A strip is clamped to a frame by ball-jointed grips. The interstand tension in the rolling direction is simulated by a lever system. The residual stress distribution is then simulated by thermal stress induced by a local heating system made of infrared emitters. In addition of the usual force, grip-to-grip displacement and thermocouples measurements, full-field measurements of the temperature and of the out-of-plane coordinate are set up.

The choice of thermal stress is promoted by the fact that thermal buckling is well established since the late 1950's, see for example the review articles of [11, 12]. Thermal buckling experiments can be found on beams [13], on uniformly heated [14] or non uniformly heated [15] shells and on plates made of metal [16, 17] or composite [18]. As buckling is of concern, a common point of all these experimental studies is the need to take specific care of the boundary conditions and the mid-surface imperfections to analyze the tests. These conditions are met in the present study by the setup of full-field measurements.

The paper is organized as follow. The experimental setup is first presented. Then, the results of a wavy edge test are analyzed in the case of "manifested" flatness defects (ie flatness defects during the tension of the strip). Eventually, a finite elements analysis demonstrates the capability of the test for numerical models validation.

1. EXPERIMENTATION

1.1. EXPERIMENTAL SETUP

Fig. 3 shows the custom experimental setup.

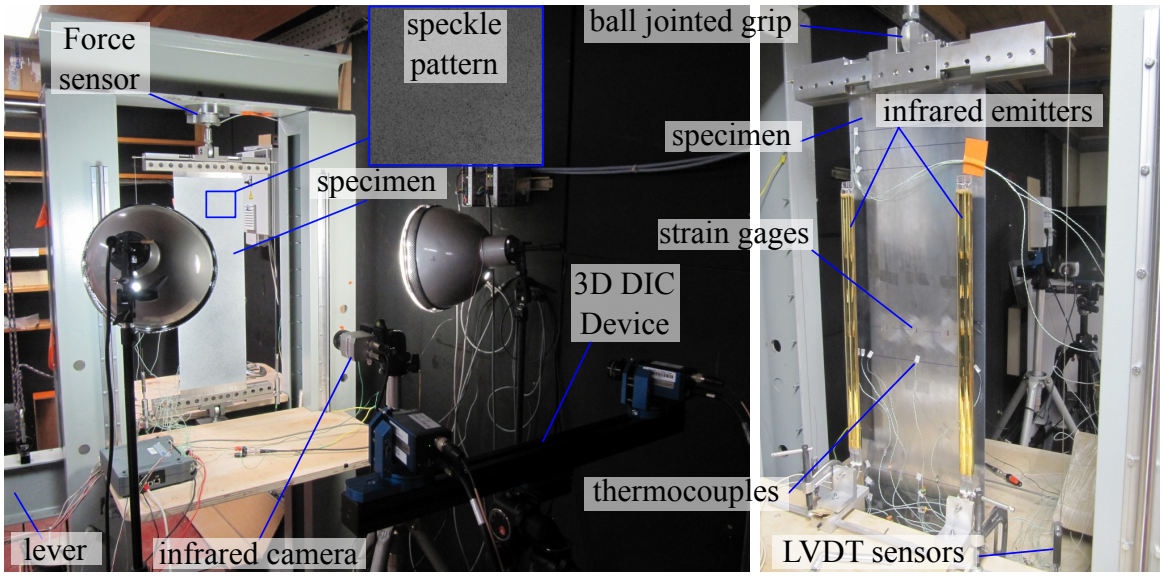

a) Full field measurements face b) Heated face

Fig. 3: Experimental setup

The specimen (Fig. 4) are cut off from a rolled plate made of middle carbon steel by a shearing machine. Its length is 800mm (Transverse direction), its width 230mm (Rolling direction), and its thickness varies in the y direction between 0.292 at the edges and 0.300 at the center. The mechanical properties of the steel at ambient temperature are listed in table 1.

TABLE 1: Mechanical properties for different angle α from the rolling direction

α ^oC	Young modulus E GPa	Poisson ratio ν	Yield stress $\sigma_{0.2}$ MPa
0	205.3	0.267	436.1
90	211.5	0.266	415.6
45	200.3	0.306	410.6

The specimen is clamped to a frame by ball-jointed grips. The inter-grips length is 731mm long. The "uniform" interstand tension is simulated by a lever system. The force is measured by a 33kN nominal load cell. The grip-to-grip displacement is measured by two LVDT sensors. The uniformity of the longitudinal stress σ_{yy} over the width of the specimen (x direction) is obtained from the measurement of strain gages depicted as G_i in Fig. 4.

In addition to the uniform tension, the residual stress distribution is simulated by thermal stress. To create thermal stress in absence of clamped boundary conditions, a two dimensional thermal gradient is needed. Hence, a local heating is applied in the region where compressive stress is wanted

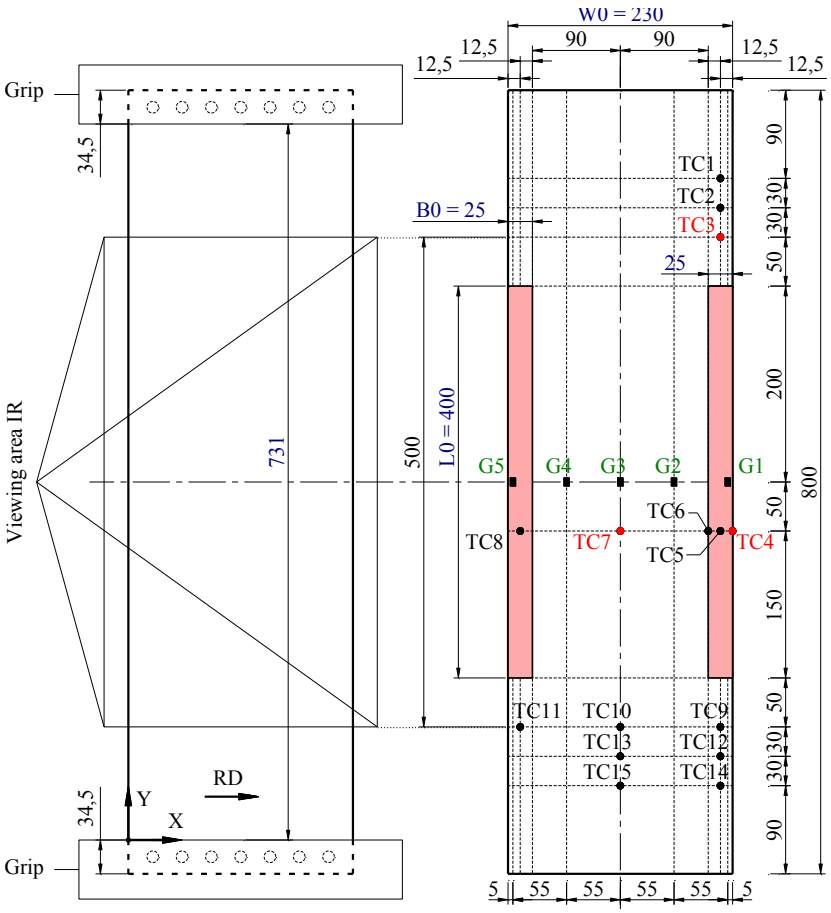

Fig. 4: Specimen, viewed from the infrared camera

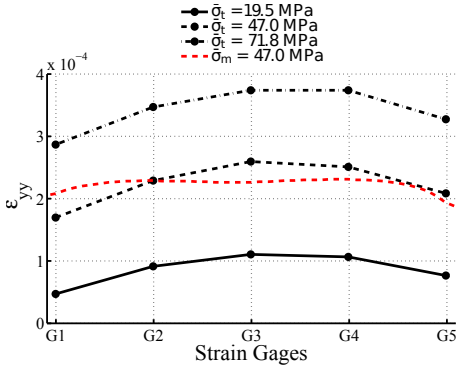

Fig. 5: Longitudinal strain over the width of the specimen, $\bar{\sigma}$ corresponds to the mean stress level, subscripts $._t$ and $._m$ corresponds to test and modeling respectively

by quartz infrared emitters (heated length 400mm, nominal wattage 2480W). In the present case, to simulate wavy edge, the emitters are set up at the edges (Fig. 4). Two regions of the heated surface (width B0=25mm, length L0=400mm, red in Fig. 4) are mat black painted in order to maximize the absorption of the radiation whereas the cold part of the heated surface is polished to minimize it (Fig. 3). Since the sheet is thin, the main source of energy dissipation is free convection. The tests are not quasi-static since it is not expected that the thermal steady state is to be reached. The heating is set up so that high thermal gradients are reached, so the heating speed is higher than the heat diffusion speed in the cold regions.

The temperature is locally measured by type K thermocouples (wire diameter 0.3mm). The thermocouples, TC_i in Fig. 4, are spot-welded on the surface. As the plate is thin, the thermocouples wires are beat out (thermal inertia minimization) and an heat insulation adhesive is sticked over them (convection minimization) to minimize measurement systematic errors. The full-field of temperature is measured by an infrared camera (resolution 382×288 pix, maximum measurement frequency 80Hz). The temperature is averaged over $1 - 1.5mm^2$ patterns. The infrared camera accuracy is $\pm 2^oC$. Some thermocouples are spot-welded in the viewing area of the infrared camera. They are used to set up and control the emissivity parameter. Some other thermocouples are spot-welded outside the viewing area, they enable a check of the linear extrapolation of the temperature in this region.

Eventually, a full-field measurement of the out-of-plane z-coordinate is measured by three-dimensional digital image correlation (3D DIC) [19, 20] using VIC 3D commercial software. The resolution of the cameras is 2048×2048 pix. An high estimation of the error is 0.05 boxel (in our case 0.02mm). Hence, a mid-surface imperfection of the tenth of the thickness can be recorded with this setup. A gray level random pattern is needed for 3D DIC. It is achieved by spraying high temperature (600^oC)

mat black and white paints on the full-field measurement surface (Fig. 3).

All the measurements including 3D DIC and the infrared camera are synchronized at 5Hz by a signal generator.

1.2. MANIFESTED WAVY EDGE DEFECTS TEST

The first step of the test is the measurement of the mid-surface imperfections by 3D DIC for different uniform tensions (ie. before thermal loading). Fig. 6 shows the mid-surface imperfections for a mean stress level $\bar{\sigma}$ of 1.5MPa. The X-coordinate is normalized by the width of the specimen W0=230mm, the Y-coordinate is normalized by the length of the black-painted region L0=400mm, the Z-coordinate is normalized by the mean thickness of the specimen T0=0.297mm. The specimen is quite flat at the center but it has very bent edges. Fig. 9 shows it for a 47MPa mean stress level that corresponds to the mechanical loading set up during the thermal step. It can be seen that the tension tends to flatten the edges. A small torsion of the specimen can also be observed. Due to the very small torsional stiffness of the specimen, the alignment of the ball-jointed grips is hard to set up. But, this small torsion has negligible influence on the buckling as it has no correlation with the buckling modes. Initial waves of smaller amplitude can be seen in Fig. 20, points (1) in a) and c). As they are modal, they have much more influence on the buckling. During the same step, the uniformity of the longitudinal stress over the width is recorded by the strain gages (Fig. 5). Tension is higher in the center than at the edges which agrees with the bent edges surface measured by 3D DIC.

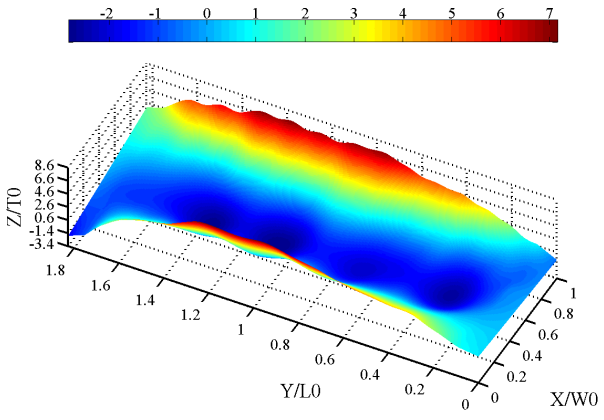

Fig. 6: Initial imperfections for $\bar{\sigma} = 1.5MPa$

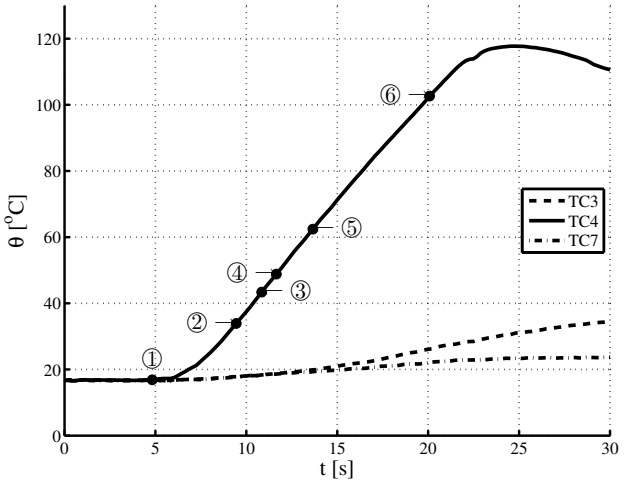

Fig. 7: Temperature vs time for thermocouples TC3, TC4, TC7

The second step is the thermal loading of the specimen. Fig. 7 shows the thermocouples measurements of TC3, TC4 and TC7. Their location is depicted in red in Fig. 4. TC3 and TC7 are in the cold region of the specimen. TC4 is in the center of the right edge in the right side of the heated region. The points 1 to 6 corresponds to Fig. 8 to 19. They show the thermal field and the normalized out-of-plane coordinate field at different times of the heating. It can be seen that high 2D thermal gradients are obtained during the test.

Fig. 11 shows the two first buckling half-waves in the left edge. They are depicted by two arrows. The amplitude of the half-waves increases until the formation of a new half-wave in the same edge (Fig.

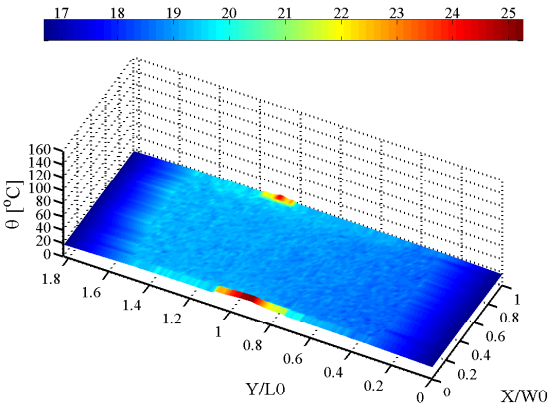

Fig. 8: IR : point 1

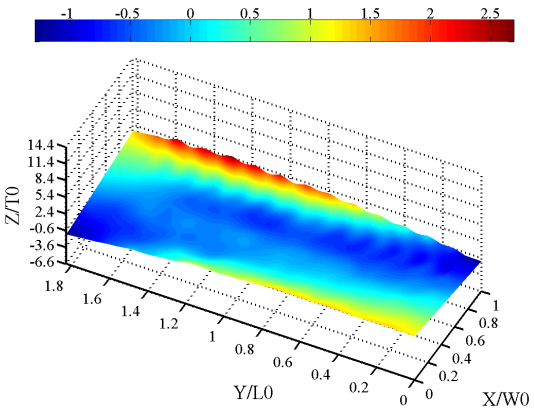

Fig. 9: DIC : point 1

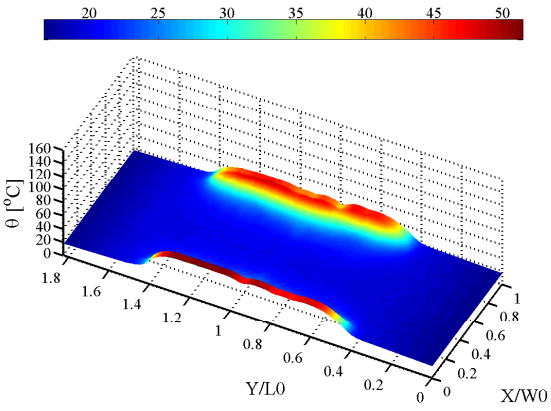

Fig. 10: IR : point 2

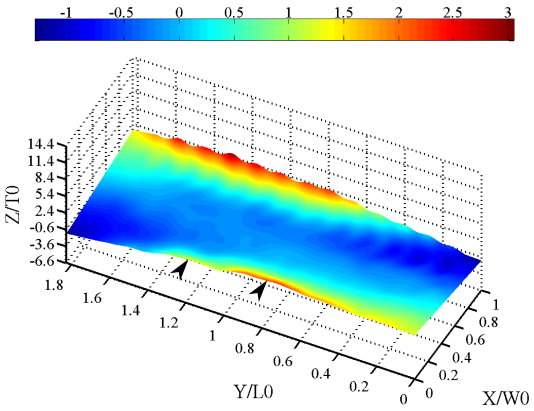

Fig. 11: DIC : point 2

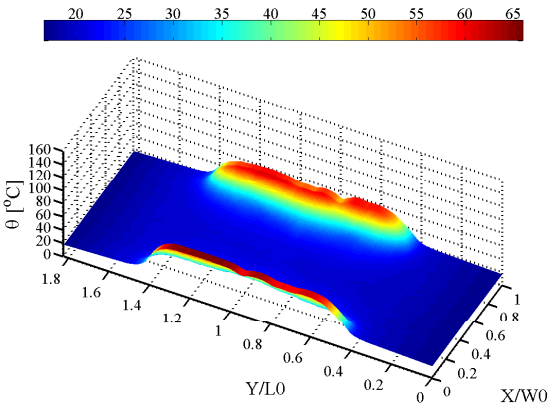

Fig. 12: IR : point 3

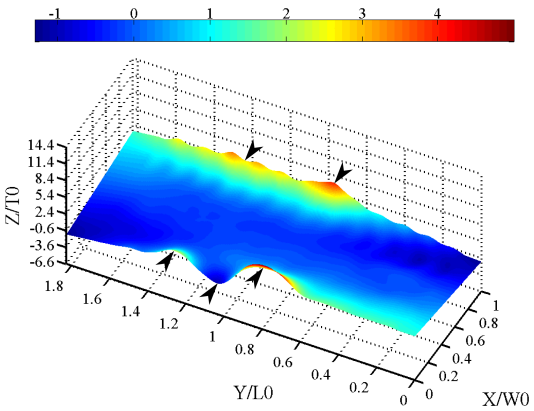

Fig. 13: DIC : point 3

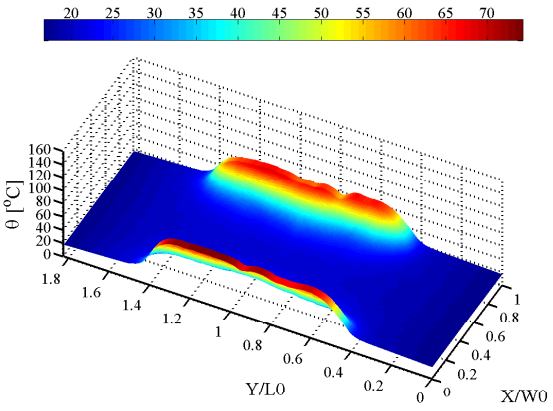

Fig. 14: IR : point 4

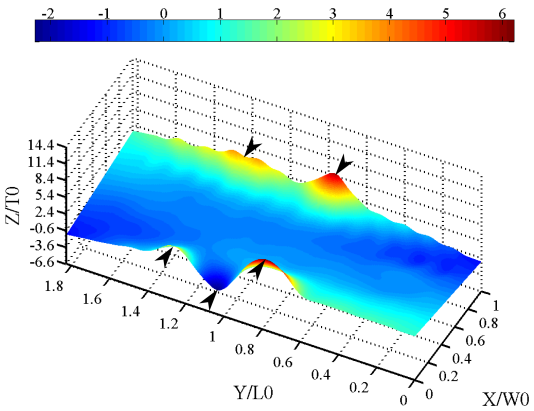

Fig. 15: DIC : point 4

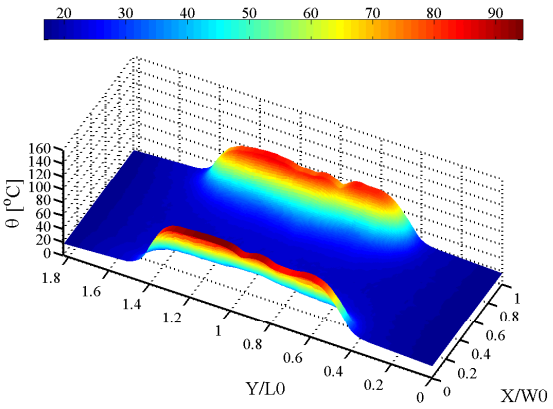

Fig. 16: IR : point 5

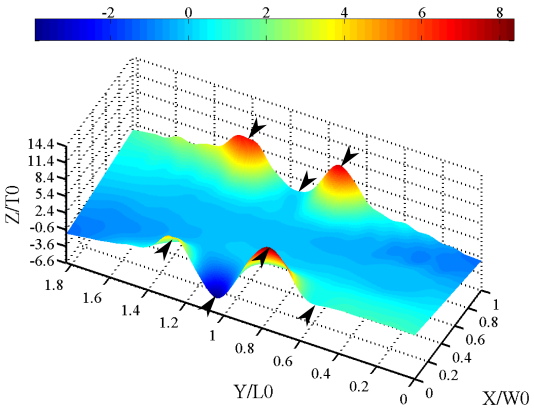

Fig. 17: DIC : point 5

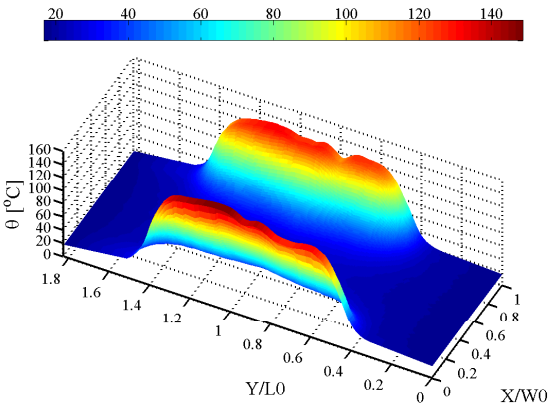

Fig. 18: IR : point 6

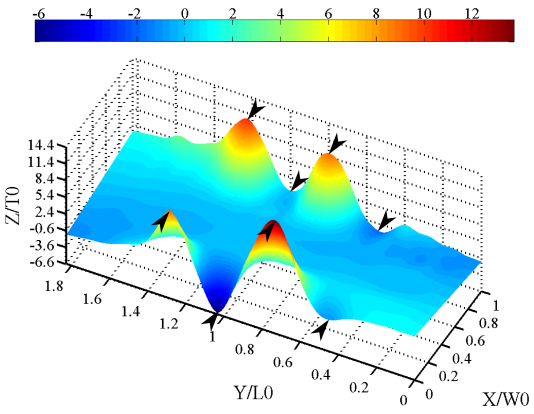

Fig. 19: DIC : point 6

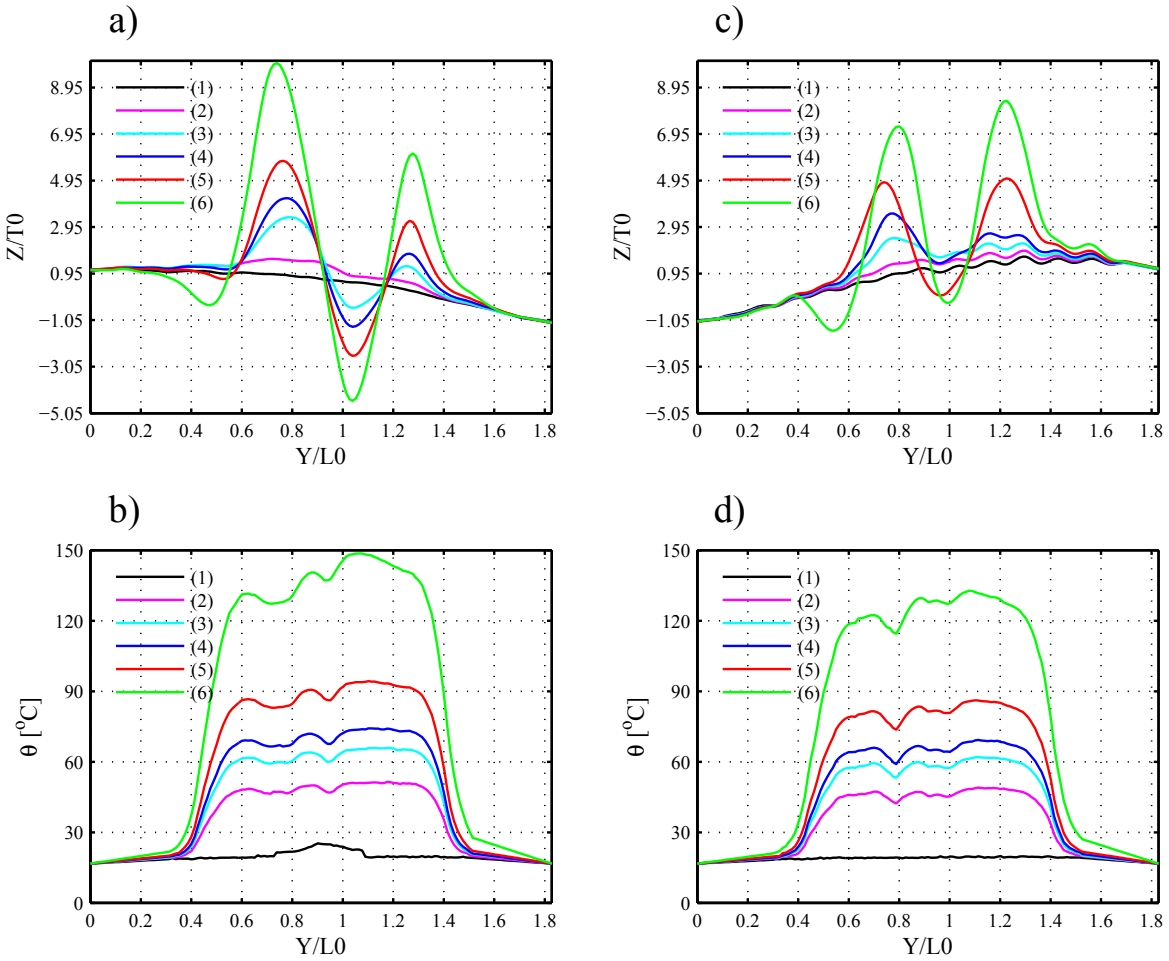

Fig. 20: Zoom on two generatrix for different times, a) Z-coordinate for x=15mm, b) Temperature for x=15mm, c) Z-coordinate for x=215mm, d) Temperature for x=215mm

13). At the same time, two buckling half-waves appear at the right edge. In Fig. 15, the increase in temperature results in the increase in the amplitudes of the existing half-waves. In Fig. 17, a bifurcation from mode 2 to mode 3 can be observed in the right edge whereas a bifurcation from mode 3 to 4 occurs in the left edge. The bifurcation from mode 3 to 4 in the right edge can be seen in Fig. 19. Fig. 20 shows the temperature profile and the normalized Z-coordinate profile along two symmetrical longitudinal generatrix at x=15mm (left edge) and x=215mm (right edge). The bifurcation from the mode with 3 half-waves to the mode with 4 half-waves can be clearly seen between 4 and 5 for the left edge and between 5 and 6 for the right edge. The loss of thermal uniformity (especially for the left edge) for times 5 and 6 can be explained by the local distance reduction between the plate and the infrared emitters due to the buckling. It can be clearly seen in Fig. 20 that the abscissa of the maximum temperature matchs the abscissa of the minimum of the normalized Z-coordinate profile. The delayed buckling of the right edge is due to a non symmetrical thermal loading. The small gaps in the temperature profile (for instance at Y/L0=0.8 in Fig. 20 d)) is the consequence of the presence of thermocouple PFA insulated wires that prevent the heat flux to reach the heated surface.

2. FINITE ELEMENTS SIMULATION

The previous test is simulated using the commercial software ABAQUS STANDARD 6.10-2. The inter-grips part of the specimen ($731\times230mm^2$) is meshed with 6716 reduced integration 4 nodes linear shell elements (S4R). A constant thickness of 0.297mm is assigned to the section. The mid-surface imperfections of Fig. 6 are taken into account as the initial ones. The material is considered as isotropic elastic with Young modulus E=205.7GPa and Poisson's ratio ν=0.28. A constant dilatation coefficient is chosen α=1.2 $10^{-5}K^{-1}$. The boundary conditions are simulated by a kinematics coupling constraint between the nodes of the top and bottom edges and the centers of the two ball joints as reference points. The minimum distance between the edges and the reference points is 65.86mm. The X and Z translations are blocked on both reference points. The Y-rotation is also blocked to prevent the calculation from numerical instabilities. In addition, the Y translation of the top reference point is blocked. A simple static calculation is performed with the non linear geometric mode (nlgeom). It is divided in two steps.

The first step corresponds to the application of the mechanical loading. This step is critical because it determines the initial mid-surface imperfections prior to the thermal loading. A stabilization procedure is needed to prevent numerical instabilities with the parameters stabilize and allsdtol. These parameters have a high influence on the longitudinal strain ϵ_{yy} profile over the width of the specimen (Fig. 5) and on the mid-surface imperfections. The best set is stabilize=0.0002 and allsdtol=0.05. Fig. 21 shows the normalized Z-coordinate profile along a line in the Y-direction at x=15mm and x=215mm. As can be seen in these figures, the mid-surface imperfections are not perfectly reproduced. The boundary conditions prevent the small torsion of the plate and results in a shift in Z-direction in Fig. 21. It is not critical as it does not correspond to a buckling mode. However, at a smaller scale, the initial waves are not exactly reproduced especially for the profile x=15mm.

The second step corresponds to the application of the experimental thermal loading via a fortran subroutine UTEMP. Fig. 22 to 24 present the results of the normalized Z-coordinate along the lines a) x=15mm and b) x=215mm for times 2, 4, 6. It is recalled that no bifurcation calculation is performed here, a simple static analysis is done. The comparison with the experiments are quite good in terms of modes and amplitude even if some differences can be analysed here. For the profile at x=15mm, the influence of the mid-surface imperfections can be clearly seen. It induces in Fig. 22 a) and 23 a) a little shift in Y-coordinate of the half-waves optimum and a shorter half wave length. However, as can be seen in Fig. 24 a), the bifurcation from the mode with 3 half-waves to 4 half-waves is well simulated. As for the profile at x=215mm, times 2 and 4 (Fig. 22 b) and 23 b)) are very well reproduced as the initial mid-surface imperfections are well reproduced. However, the bifurcation from mode 3 to 4 in Fig. 24 b) is not exactly captured. A bifurcation analysis may be needed to capture it.

3. CONCLUSIONS

In the framework of rolling flatness defect simulation, a thermal buckling test is presented for buckling models validation purpose. Manifested wavy edge flatness defects are experimentally simulated with accurate full-field measurements of the temperature and the out-of-plane coordinates. The residual stress responsible for the buckling is simulated by thermal stress. A simple FE static analysis is performed to demonstrate the legitimacy of the test for models validation.
The test has been designed so that other stress distributions can be simulated (center waves defects for example...). Moreover, latent flatness defects can also be simulated when the mechanical loading, which simulates the interstand tension, is released during the test.

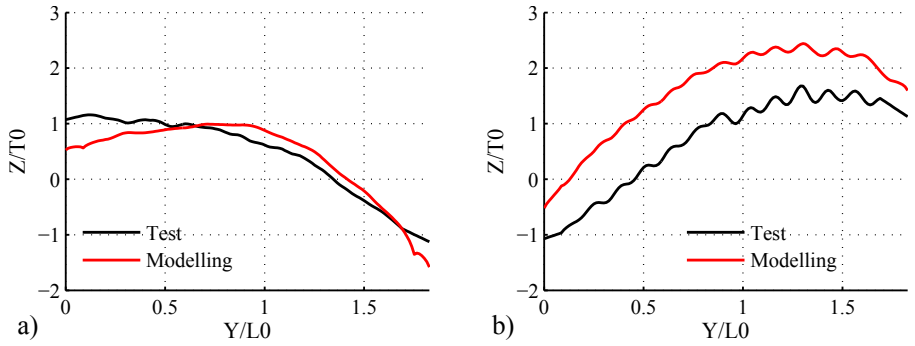

Fig. 21: Comparison of the normalized Z-coordinate for the generatrix a) x=15mm and b) x=215mm. Point 1.

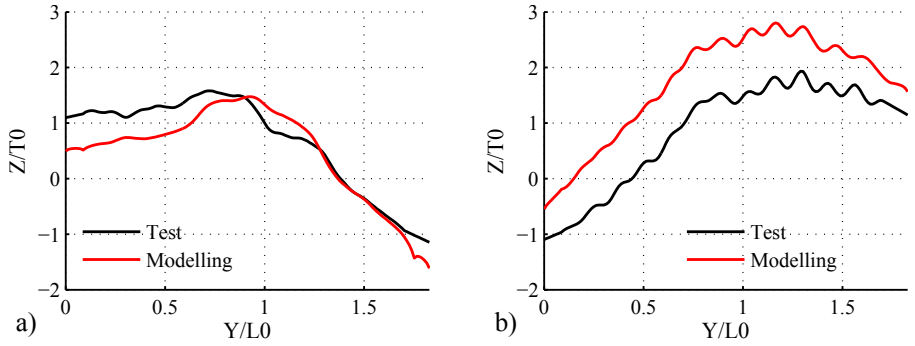

Fig. 22: Comparison of the normalized Z-coordinate for the generatrix a) x=15mm and b) x=215mm. Point 2.

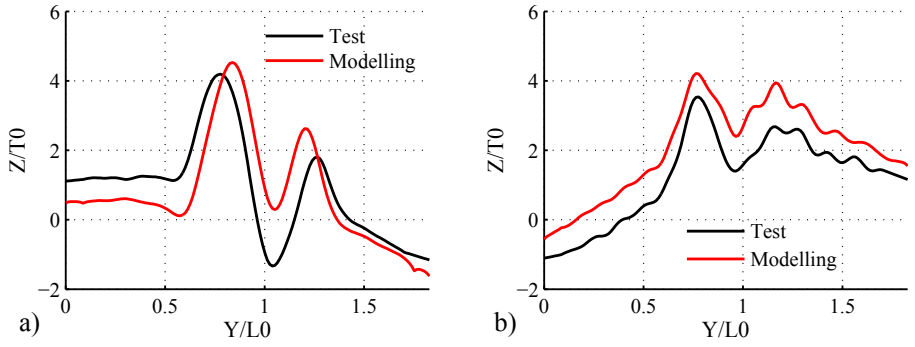

Fig. 23: Comparison of the normalized Z-coordinate for the generatrix a) x=15mm and b) x=215mm. Point 4.

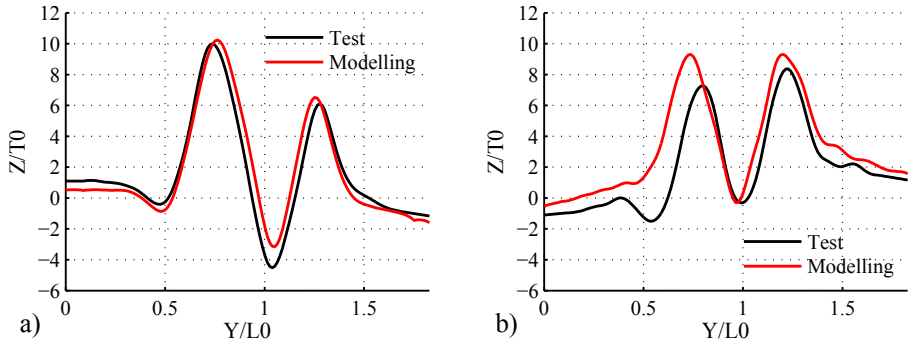

Fig. 24: Comparison of the normalized Z-coordinate for the generatrix a) x=15mm and b) x=215mm. Point 6.

ACKNOWLEDGMENTS

The study was performed in the framework of the ANR PLATFORM # 2012-RNMP-019-06. The authors would like to acknowledge all the participants of the project : ArcelorMittal, CEA, CEMEF-MINES, PARISTECH, Constellium, Ecole Centrale of Paris, INSA Lyon and Paul Verlaine university of Metz. Thanks to Dr P. Chantrenne, Dr F. Morestin and Dr M. Coret for the benefit of helpful discussions on this work.

REFERENCES

1) S. ABDELKHALEK, P. MONTMITONNET, N. LEGRAND and P. BUESSLER, Int. J. Mech. Sci., (2011), p.15.
2) C. COUNHAYE, Ph.D Thesis, Université de Liège, (2000), p.237.
3) F. FISCHER, F.G. RAMMERSTORFER, N. FRIEDL and W. WIESER, Int. J. Mech. Sci., (2000), p.24.
4) F.G. RAMMERSTORFER, F. FISCHER and N. FRIEDL, J. Appl. Mech., (2001), p.6.
5) F.D. FISCHER, F.G. RAMMERSTORFER and N. FRIEDL, J. Appl. Mech., (2003), p.7.
6) S. ABDELKHALEK, H. ZAHROUNI, M. POTIER-FERRY, N. LEGRAND, P. MONTMITONNET and P. BUESSLER, ESAFORM, (2009), p.4.
7) N. DAMIL and M. POTIER-FERRY, Journal of the Mechanics and Physics of Solids, (2010), p.15.
8) D. RODDEMAN, J. DRUKKER, C. OOMENS and J. JANSSEN, J. Appl. Mech., (1987), p.4.
9) P. MONTMITONNET, Comput. Methods Appl. Mech. Engrg., (2006), p.22.
10) A. HACQUIN, P. MONTMITONNET and J.-P. GUILLERAULT, Journal of Materials Processing Technology, (1996), p.8.
11) T.R. TAUCHERT, Applied Mechanics Reviews, (1991), p.347.
12) E.A. THORNTON, Applied Mechanics Reviews, (1993), p.485.
13) J. RODRIGUES, I. CABRITA NEVES and J. VALENTE, Fire Safety Journal, (2000), p.22.
14) B. ROSS, N.J. HOFF and W.H. HORTON, Experimental Mechanics, (1966), p.9.
15) D. BUSHNELL and S. SMITH, AIAA Journal, (1971), p.8.
16) E.A. THORNTON, M.F. COYLE and R.N. MCLEOD, Journal of Thermal Stresses, (1994), p.22.
17) K.D. MURPHY and D. FERREIRA, International Journal of Solids and Structures, (2001), p.16.
18) M. AMABILI and M.R.S. TAJAHMADI, Proc. I. Mech. E. Part C : J. Mechanical Engineering Science, (2012), p.9.
19) T. CHU, W. RANSON, M. SUTTON, Experimental Mechanics, (1985), p.13.
20) P. LUO, Y. CHAO, M. SUTTON and W.-H. PETERS, Experimental Mechanics, (1993), p.10.